RESEARCH ARTICLE

Designing of 10 Wt. % Graphite Particulate Hot Forged AA7075 Composites and its Loss Factor Analysis

N.B. Dhokey[1,*], A.G. Jadhav[1], S.S. Nimbalkar[1], V. Nimbalkar[2]

[1]Department of Metallurgy and Material Science, College of Engineering Pune 411005, India
[2]Naval Materials Research Laboratory, DRDO, Ambernath 421506, India

*Corresponding author: Email: nbdhokey@yahoo.co.in; Tel.: (+91) 9284013245

DOI: 10.5185/amlett.2021.041623

The composite material is an emerging opportunity for improving the loss factor. In the present context, AA7075 was fabricated in induction furnace using elemental addition such as Zn, Mg and Cu and ex-situ reinforcement of 10wt. % graphite particulates with three types of composites viz 3 to 10 µm (C1), 53 to 66 µm (C2) and 106 to 150 µm (C3). The melt was poured at 780°C and cast into the steel mold then hot forged at a strain rate of 3- 5x10-3 s-1 in three stages with net cross-section reduction in the range of 30-33%. Solutionizing at 470°C was followed by artificial aging at 120°C. Characterization was carried out by SEM and DMA at two selected frequencies 0.1Hz and 1Hz over the temperature range of 30 to 250°C. Significant improvement in storage modulus (E') and loss modulus (E") noticed in C2 as compared to the C1, C2 and monolithic alloy. A threshold value of the volume to the surface of graphite reinforcement has arrived for an improved loss factor. A generalized experimental model formulated to account for 12 influencing parameters and the significance of damping capacity with the response to graphite content has been established.

Introduction

Aluminum alloy, Al-Zn-Mg-Cu (AA7075) is suitable for the various age-hardening heat treatment processes. It is one of the secondary processing alloy and ever-increasing usage in structural applications such as automobile, aerospace, and marine industries, due to its high strength to weight ratio and excellent stiffness [**1, 2**]. Aluminum alloy-based metal matrix composites (MMC) are natural in processing and it is economical and easy in fabrication by liquid metallurgy route [**3**]. Structural applications are frequently subjects to mechanical vibration. The monolithic metals and alloys do not possess high damping capacity with high strength to weight ratio together [**4**]. However, high damping capacity the MMC processing may be effectively utilized, firstly by incorporating high damping capacity reinforcement, and secondly the modification of microstructure can result in an appropriate source to dissipate energy in the materials. Consequently, it will eliminate the need for special energy absorber or massive dampers [**5**].

Accordingly, studies are available on the improvement of the damping capacity of monolithic metals by introducing a new phase through reinforcement. Zhang *et. al.,* [**6**] have studied the effect of different ceramic particulates on damping capacity such as SiC, Al_2O_3, and graphite as reinforcement in the aluminum matrix. The intrinsic damping capacity of the graphite (0.013) is high as compared with SiC (0.05) and Al_2O_3 (0.005), which enhances the damping property of the matrix alloy. Rohatgi *et. al.,* [**7**] have demonstrated that the damping capacity of aluminum alloy having the dispersion of 10 vol.% graphite particulate composites by stir casting and concluded that the improvement in damping capacity of the MMC than the monolithic alloy. However, Zhang *et. al.,* [**8**] have investigated that the damping capacity of the aluminum MMC reinforced with graphite particulates has shown increased damping capacity two to three times over that of as-received aluminum alloy. The defects in MMCs generated due to the second phase particles such as dislocation and grain boundaries play a vital role in such a way that it moves slightly at an interface concerning each other during vibration and hence enhances the internal friction that helps to dissipate energy [**9**]. D.L. Chung [**10**] has pointed out that the damping capacity is depends on its evaluating parameters such as applied frequency, heating rate, strain amplitude, and temperature. However, the damping capacity of the hybrid MMCs is enhanced at lower test frequency [**11,12**].

Furthermore, Wu *et. al.,* [**13**] have reviewed the effect of size of reinforcement particle and shown that smaller diameter particles occupy more volume, thereby generates more void defects and thus improves the damping capacity. Similarly, Wei *et. al.,* [**14**] stated that the microscopic graphite particulates reinforced MMCs have shown promising improvements in the damping capacity. As observed by, Wei *et. al.,* [**15**] have studied that the

reinforcement of graphite particulates for the given particulates size range (500-1500μm) to the commercial Al was showed to provide increased damping capacity of composite over matrix metal in the 0.5 to 3Hz frequency range. The development of the aluminum MMC has been employed for the vibrational damping due to its inherent viscoelastic nature. A comparative loss factor analysis of the published work has been analyzed as indicated in Appendix-A.

Improving the damping capacity of material by reinforcing particulates is multi-dimensional parameters. There is limited understanding available in the published literature on designing new composites. In this work, high strength Al7075 has been chosen to reinforce with graphite particulates which is one of the novelties to study damping capacity. In the present work analyzes the effect of varied particulate sizes of graphite reinforcement on the damping behavior of hot forged monolithic alloy and its graphite-reinforced composites. Besides, the generalized experimental model has been proposed, to established mathematical correlation.

Formulation of Generalized Experimental Model (GEM) for loss factor analysis

In the present work, effect of various material and test parameters on damping capacity (tan δ) has been identified. The loss factor or damping capacity is a ratio of loss modulus to storage modulus. The total 12 parameters are considered as shown in **Table 1** and **Table 2**. Sr. no. 1 to 7 are the materials parameters and sr. no. 8 to 12 are the DMA testing parameters in Table 1. The tan δ is a function of these parameters, and the relation among them is solved by using the Buckingham's Pi theorem and it is expressed by Eq. (1). It is stated that dimensionally homogeneous equation involving 'n' variables and 'm' primary or fundamental dimensions can be reduced to a single relationship among n-m independent dimensionless products that have been elaborated in Appendix.

The loss factor (tan δ) using the Buckingham's Pi theorem can be expressed as,

$$\tan\delta = f(\text{material parameters, test parameters})$$

$$\tan\delta = f(\rho_c, F_m, P_p, E_c, R_d, t_a, H_b, a, f, t, T, \lambda) \quad (1)$$

The resulted final form of equation for loss factor (tan δ) is,

$$\tan\delta = \varphi\,[(\rho_c . f^5 . a^2 . H_b . t_a . t . T . F_m . P_p . R_d) / (E_c^2 . \lambda)]^A \quad (2)$$

$$\tan\delta = \varphi\,(Z)^A \quad (3)$$

Terminology

Loss Factor (tan δ)

The loss factor (tan δ) is expressed as a ratio of loss modulus (E") to storage modulus (E').

Dimensionless parameter (Z)

From the equations, (2) and (3), it is clear that the term Z is a ratio and product of multiple parameters i.e., material as well as test parameters listed in **Table 1**. This term is resulted from the relationship of all 12 parameters such as density (ρ_c), frequency (f), strain amplitude (a), bulk hardness (H_b), aging time (t_a), test time (t), temperature (T), matrix fraction factor (F_m) i.e., volume percentage of matrix in composite, porosity (P_p), percentage reduction in forging (R_d), heating rate (λ) and elastic modulus of material (E_c). The most dominant parameters are frequency (f^5), elastic modulus (E_c^2) and strain amplitude (a^2). Any interaction amongst the variables is configured in Z is reflected in terms of exponent A.

On taking logarithm to equation 3, the intercept on the y-axis accounts for intrinsic behavior of material referred to as Φ and interaction of all 12 variables manifest in the form of exponent A. These characteristic constants are obtained by conducting experiments, graph plotting and solving the equations.

Table 1. Abbreviations of symbol and their dimensional forms GEM.

Parameters	Symbols	Units	Dimensionless unit
Density	ρ_c	Kg/m^3	M^1L^{-3}
Matrix Fraction Factor	Fm	–	–
Porosity	P_p	%	–
Bulk Hardness	H_b	MPa	$M^1L^{-1}T^{-2}$
Degree of Reduction in Forging	R_d	%	–
Aging Time	t_a	s	T^1
Elastic Modulus	Ec	MPa	$M^1L^{-1}T^{-2}$
Strain Amplitude	a	M	L^1
Frequency	f	s^{-1}	T^{-1}
Loading Time	t	s	T^1
Test Temperature	T	°C	θ^1
Heating Rate	λ	°C/min	$T^{-1}\theta^1$

Table 2. Some of the properties and processing parameters kept unchanged in solving GE model.

Parameters	Units	MA	C1	C2	C3
Density (ρ_c)	Kg/m^3	2835.1	2814.4	2833.9	2833.7
% reduction in forging (R_d)	%	24.28	30.86	31.26	39.74
Porosity (P_p)	%	6.12	4.44	3.77	3.78
Matrix Fraction Factor (F_m)	–	1	0.88	0.88	0.88
Hardness (H_b)	Kg/m^2	19449541	17850152	17654434	17388379

Experimental Method

Fabrication of composite

In house aluminum alloy (AA7075) and its composite reinforced with 10 wt.% graphite was manufactured by liquid metallurgy route (stir casting) using an induction furnace. All alloying elements (Zn, Mg, and Cu) were added into the melt by wrapping in aluminum foil. Cleaning flux (CEAFLUX-11) was used amounting to 1% of the total weighted metal charge to prevent the initial oxidation and refine the liquid metal. Metal-free dross was

then removed from the monolithic alloy and preheated graphite particulates with average particulate diameter size 3 to 10μm (C1), 53 to 66μm (C2) and 106 to 150μm (C3) having 99% purity was used as reinforcement **Table 3**. The molten alloy and composite were cast in rectangular mild steel mold having 45×45×120mm^3 in size. The cast rectangular bars were homogenized at 450°C for 24 hours [**16**].

Table 3. Batch coding for monolithic alloy AA7075 reinforced with 10 wt.% graphite composites C1, C2 and C3.

Sr. No.	Sample Code	Alloy and Composite Description
1	MA	Monolithic Alloy (AA7075)
2	C1	Composite reinforced with graphite particulate having size range (3 to 10μm) or (+4800 to -1250 mesh)
3	C2	Composite reinforced with graphite particulate having size range (53 to 66 μm) or (+270 to -230 mesh)
4	C3	Composite reinforced with graphite particulate having size range (106 to 150μm) or (+140 to -100 mesh)

Hot Forging

Open die hot forging was done using a Universal Testing Machine (Capacity: 60 Ton). Hot forging of cast specimens was carried out in three successive stages having a reduction of about 10% at each stage. The hot deformation temperature was maintained at 490°C for the soaking period of 2 h for the initial stage and 1h for the remaining two stages, ASM Metal Handbook [**17**]. A rectangular cast specimen was hot deformed at the strain rate of 3×10^{-3} s^{-1} to 5×10^{-3} s^{-1} all along the length of the specimen. The average overall reduction in cross sectionals areas for all specimens was obtained in the range of 30 to 33% and an increase in length was 40 to 42%.

Metallography

The specimens were polished using emery paper (series 800, 1000, 1500 and 2000 grit) for microstructural observations. The final polishing was done on a fine 2000 grit paper to obtain a scratch-free finish followed by lapping with brasso. The specimen etched using Keller's reagent (2ml HF + 3ml HCl + 5ml HNO_3 + 190ml H_2O) for 40-45 sec, rinsing in acetone to remove the leftover chemical residues and then dried, ASM Metal Handbook [**18**]. The microstructure was observed using an inverted optical microscope and field emission scanning electron microscope (Make Carl Zeiss, Germany) to reveal microstructural constituents. Whenever possible, SEM-EDS micro chemical analysis was carried out at selected locations.

Heat treatment

Heat treatment was done in accordance to ASM Metal Handbook [**19**]. Solutionizing was done at 470°C for 65 minutes in presence of argon followed by water quenching and then aged in oven at 120°C for 24 hours (T6). Overall, the thermal processing is illustrated in **Fig. 1**, which is employed for specimens that are extracted for analysis of damping capacity of the materials.

Damping measurements

A Dynamic Mechanical Analyzer (DMA) instrument (Make and Model: DMA 242 E Artemis, NETZSCH) was used for measurement of the viscoelastic response of matrix alloy and composite. The rectangular specimen of 40mm in length, 7.5mm in width and 1.8mm in thickness, were extracted and machined from the hot forged and heat treatment as per **Fig. 1**. The mechanical excitation was applied in three-point bending mode at 100μm stain amplitude according to ASTM Standard [**20**]. The DMA was configured sequentially to apply dynamic loading of 2.18 N and frequency at 0.1Hz and 1Hz over the temperature range from 30°C to 250°C with a heating rate of 5°C/min. During experimentation, data were isothermally recorded for the storage modulus (E'), loss modulus (E") and damping capacity in terms of loss factor (tan δ) over each temperature step. The summary of parameters applied during DMA testing is tabulated in

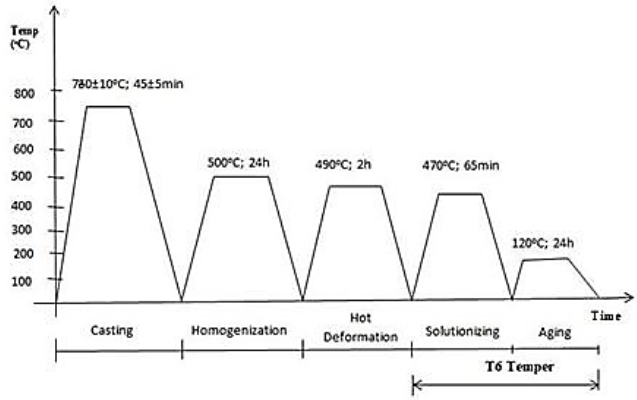

Fig. 1. Diagrammatic representation of casting, homogenization, hot deformation and heat treatment cycle.

Table 4. DMA test parameters employed for damping capacity of materials.

Sr. No.	Parameters	Units	Values
1	Strain amplitude (a)	m	0.0001
2	Aging time (t_a) (Heat Treatment Parameter)	s	86400
3	Test time (t)	s	2640
4	Heating rate (λ)	K/s	4.6333

Results and discussion

Matrix-Graphite interface

Fig. 2(a), Fig. 2(b) and **Fig. 2(c)** show microstructures of monolithic alloy and composite having different sized graphite particulates that were used. The microstructure of composite shows moderately distributed graphite particles. All specimens were hot forged at 490°C in three successive stages and then air-cooled followed by T6 temper as indicated in Fig. 1. The graphite-parent matrix interface exhibits strong bonding, free from any defects as shown in **Fig. 2**.

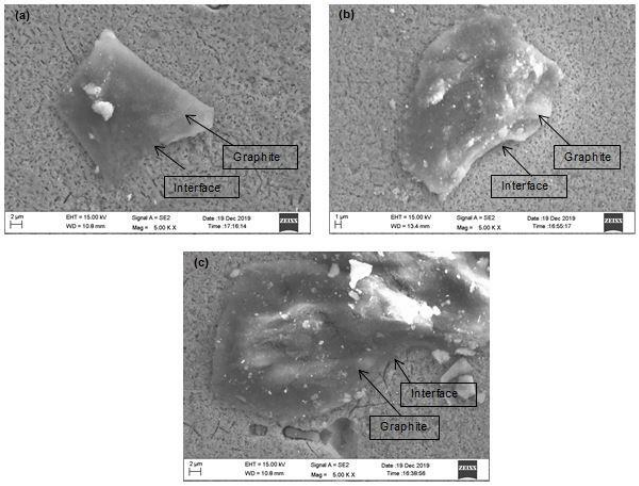

Fig. 2. SEM micrograph showing graphite matrix interface after hot forge condition for a) C1; b) C2; c) C3.

The EDS analysis of precipitates and eutectics identifies their presence in the matrix as indicated in **Fig. 3** and **Table 5**. Besides graphite particulates were analyzed by EDS for spot chemical analysis depicts the presence of aluminum traces in graphite as shown in **Fig. 4** and **Table 6**. This clearly indicates that there might be the formation of aluminum carbide due to prolonged soaking period during heat treatment as shown in Fig. 1. Thus, the overall improvement in graphite matrix interface strengthening is depicted by C2 composite.

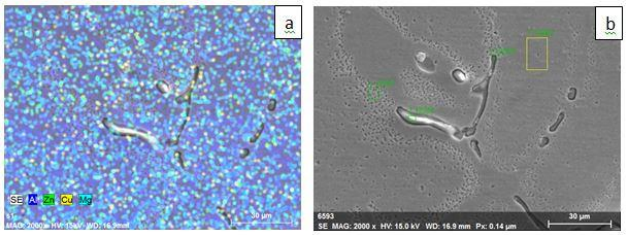

Fig. 3. Elemental mapping and SEM-EDS micrograph of MA after hot forging; a) Elemental analysis; b) SEM-EDS micrograph.

Table 5. SEM- EDS elemental mapping of MA constituents (Fig. 3(b)).

Sr. No.	Spectrum	Elements (Wt% Atom)				
		Zn	Mg	Cu	Al	Total
1	1 12056	4	3.23	5.86	86.9	100
2	1 12058	7.22	2.11	2.27	88.4	100
3	1 12059	10.41	1.99	1.6	86	100
4	1 12062	3.96	2.16	2.61	91.27	100

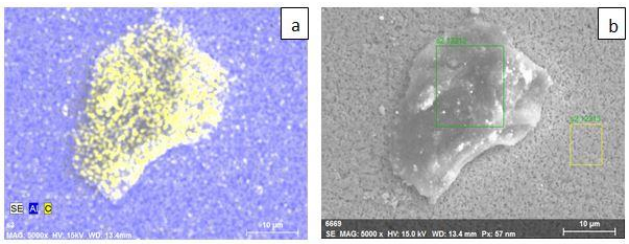

Fig. 4. Elemental mapping and SEM-EDS micrograph of **C2** after hot forging; a) Elemental analysis; b) SEM-EDS micrograph.

Table 6. SEM- EDS elemental mapping of **C2** constituents (Fig. 4(b)).

Sr. No.	Spectrum	Elements (Wt% Atom)					
		Zn	Mg	Cu	C	Al	Total
1	S2 12212	1.2	0.62	0.26	72.19	25.75	100
2	S2 12213	4.9	1.57	0.85	12.55	80.12	100

Effect of test temperature on storage modulus (E') and loss Modulus (E")

The objective of DMA testing was to compare the loss factor analysis of monolithic alloy and that of composite specimens. DMA gives values of E' (storage modulus), E" (Loss modulus), and tanδ (loss factor = E"/E') at different frequencies and over-temperature ranges starting from room temperature to 240ºC. It is evident from **Fig. 5** that the storage modulus is on the higher side at 1Hz than at 0.1 Hz. Overall, in both these frequencies, storage modulus decreases gradually with test temperature. Among the composites and MA, C2 showed higher storage modulus and whereas lowest being MA at both the frequencies. This improvement in storage modulus in C2 can be attributed to strong interfacial bonding due to aluminum carbide formation.

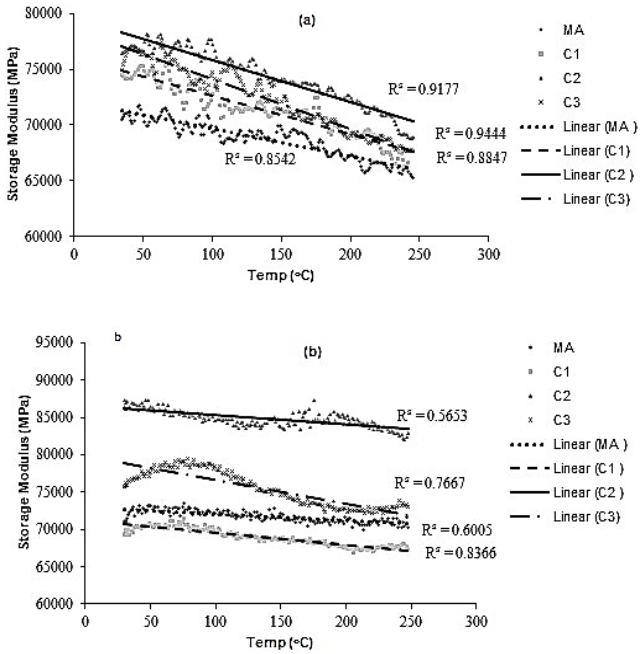

Fig. 5. Effect of test temperature on storage modulus (E') of MA and its composites at; a) 0.1Hz; b) 1Hz.

Besides, loss modulus at 0.1Hz and 1Hz increases with test temperature as evident in **Fig. 6**. At a higher frequency of 1Hz, there is an increase in loss modulus for C2 and overlapping behavior for other composites and MA. It is noticed that magnification in loss modulus at 0.1Hz is relatively less than that at 1Hz. Thus, loss modulus is on the higher side for C2 than other materials.

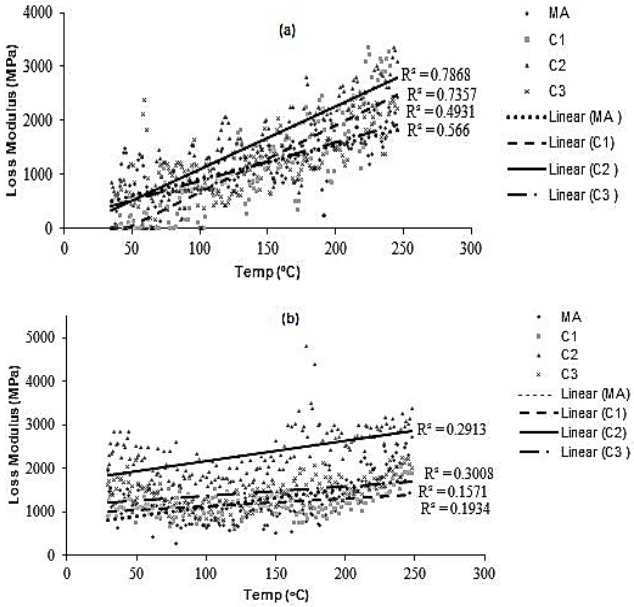

Fig. 6. Effect of test temperature on loss modulus (E") of MA and its composites at; (a) 0.1Hz; (b) 1Hz.

Effect of test temperature on loss factor (tanδ)

The loss factor or damping capacity is expressed as the ratio of loss modulus to storage modulus as depicted in **Fig. 7**. It is noted that the graphite reinforcement improves damping capacity above 100°C and it becomes appreciable beyond 200°C. Kenneth *et. al.*, [**12**] described increase in the damping capacity with the temperature is significant. Out of three sizes of graphite, reinforcement chosen, only C2 composite shows a significant rise in viscoelastic behavior as compared to C1, C3 and MA. This improved loss factor is varied from 10 to 15% in C2 as compared to MA over the entire test temperature range at 1Hz. Besides, the loss factor is low at the frequency of 0.1Hz, whereas it is significant at the higher frequency of 1Hz. Thus, overall improvement in the loss factor is evident in C2 composite, which can be attributed to improved interface graphite matrix and formation of aluminum carbide (Fig. 4). Further, this improved performance can be correlated to optimum modulus (volume to surface ratio of graphite particulate) for graphite reinforcement in C2 than that in other composites. In other word, graphite size in C2 is the threshold modulus responsible for the appreciable improvement in damping capacity or loss factor.

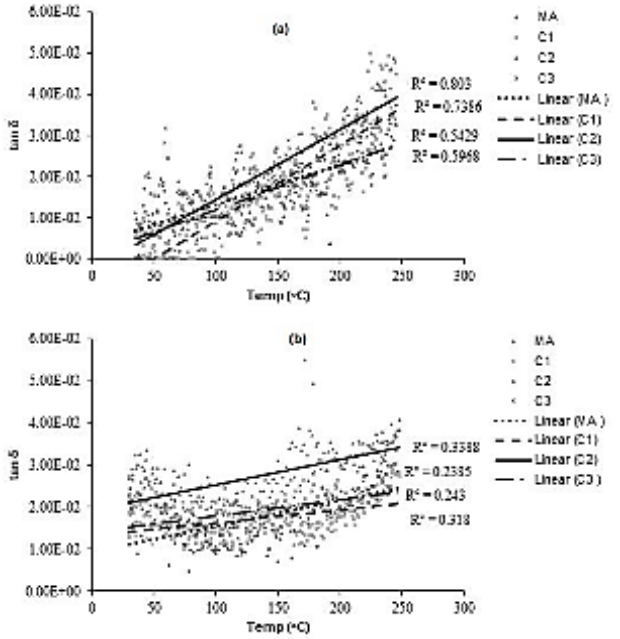

Fig. 7. Effect of test temperature on loss Factor (tan δ) of MA and its composites at; a) 0.1Hz; b) 1Hz.

Table 7. Summary of tanδ and other forms of dimensionless number.

Stages of Test	Temp. T (K)	Test Frequency f (1/s)	MA			C1			C2			C3		
			tan δ	Ec (Kg/m²)	Z	tan δ	Ec (Kg/m²)	Z	tan δ	Ec (Kg/m²)	Z	tan δ	Ec (Kg/m²)	Z
1	323	0.1	0.0155	7.199E +09	2.514E -14	0.0011	7.616E +09	1.661E -14	0.0068	7.853E+ 09	1.338E -14	0.0106	7.772E +09	1.715E -14
		1	0.0182	7.412E +09	2.372E -09	0.0164	7.177E +09	1.870E -09	0.0263	8.814E+ 09	1.062E -09	0.0209	7.924E +09	1.649E -09
2	373	0.1	0.0104	7.093E +09	2.991E -14	0.0079	7.366E +09	2.050E -14	0.0151	7.783E+ 09	1.573E -14	0.0114	7.547E +09	2.100E -14
		1	0.0116	7.368E +09	2.771E -09	0.0157	7.111E +09	2.200E -09	0.0211	8.646E+ 09	1.274E -09	0.0132	7.964E +09	1.886E -09
3	423	0.1	0.0181	7.054E +09	3.429E -14	0.0167	7.251E +09	2.399E -14	0.0203	7.541E+ 09	1.900E -14	0.0181	7.359E +09	2.504E -14
		1	0.0144	7.310E +09	3.193E -09	0.0175	6.996E +09	2.577E -09	0.0252	8.605E+ 09	1.459E -09	0.0183	7.614E +09	2.340E -09
4	473	0.1	0.0209	6.827E +09	4.093E -14	0.0238	7.056E +09	2.833E -14	0.0307	7.359E+ 09	2.231E -14	0.0211	7.053E +09	3.049E -14
		1	0.0205	7.251E +09	3.629E -09	0.0176	6.888E +09	2.973E -09	0.0315	8.657E+ 09	1.612E -09	0.0210	7.403E +09	2.768E -09
5	503	0.1	0.0263	6.752E +09	4.451E -14	0.0408	6.858E +09	3.190E -14	0.0377	7.168E+ 09	2.500E -14	0.0283	6.975E +09	3.315E -14
		1	0.0289	7.242E +09	3.869E -09	0.0234	6.891E +09	3.159E -09	0.0346	8.498E+ 09	1.779E -09	0.0254	7.416E +09	2.933E -09

Analysis of GEM

In the foregoing discussions, the effect of individual parameters like test temperature on storage modulus/ loss modulus/ tan δ have been analyzed to realize the degree of improvement for various composites fabricated in this work. It is observed that the effect of a single parameter gives a limited understanding of the damping behavior of the composite. Hence, an attempt has been made to derive the dimensionless parameter to describe the combined effect of influencing parameters on damping capacity. Using equation 3, the resultant summary is tabulated in **Table 7**. It is evident from **Fig. 8** to **Fig. 11** shows the relationship of log tanδ with log Z with the intercept of log Φ on the y-axis

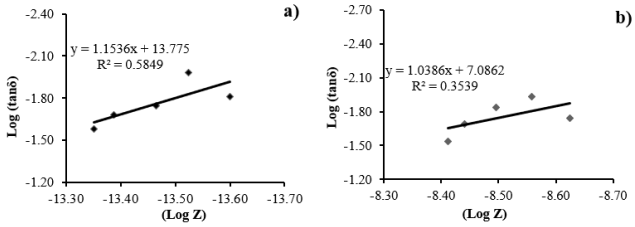

Fig. 8. Plot of Log (tan δ) vs. (Log Z) to know the value of exponent (A) and intrinsic damping (Log φ) for **MA** at; a) 0.1Hz; b) 1Hz

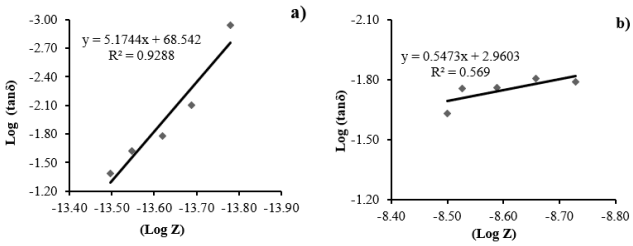

Fig. 9. Plot of Log (tan δ) vs. (Log Z) to know the value of exponent (A) and intrinsic damping (Log φ) for **C1** at; a) 0.1Hz; b) 1Hz.

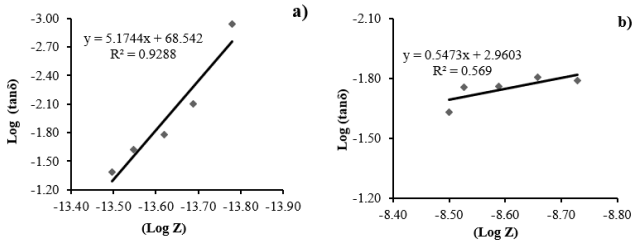

Fig. 10. Plot of Log (tan δ) vs. (Log Z) to know the value of exponent (A) and intrinsic damping (Log φ) for **C2** at; a) 0.1Hz; b) 1Hz.

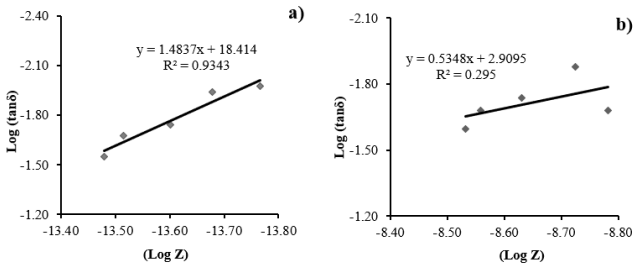

Fig. 11. Plot of Log (tan δ) vs. (Log Z) to know the value of exponent (A) and intrinsic damping (Log φ) for **C3** at; a) 0.1Hz; b) 1Hz.

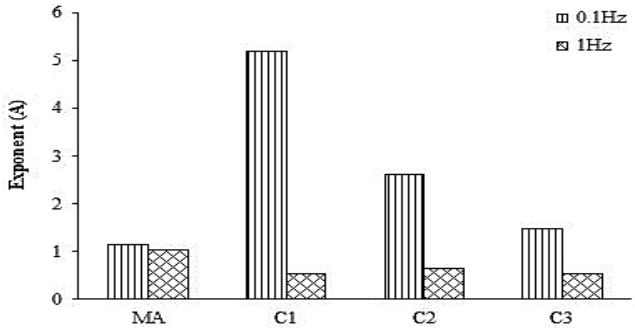

Fig. 12. Plot shows exponent (A) obtained from GEM depicts damping behavior of materials

Significance of exponent (A)

From **Fig. 12** it is clear that the exponent value for MA at 0.1Hz and 1Hz is almost the same; on the other hand, there is a huge amount of difference in exponent values of C1, C2 and C3 at 0.1Hz and 1Hz. A combined interactive dimensionless parameter Z is plotted against tan δ gives dimensionless exponent (A) as indicated in **Fig. 12** for the composites fabricated in this work. It gives clarity on the damping behavior of the material. In this work, it is noted that if A is less than 0.7, it indicates reasonably improved damping behavior for all these composites C1, C2 and C3. Since the Z parameter is the result of the other 12 influencing parameters, it provides a unique dimensionless number to each of the composites and almost this exponent indicates average behavior of that material. Moreover, exponent A does not recognize a narrow range of particulate sizes that are used in this work. In nutshell, the generalized model developed in this work provides a logical basis for the selection of improved damping capacity of the composites. Similarly, if A is greater than 0.7, then exponent A implies poor damping capacity as noted in MA alloy. Overall, the large difference in values of exponent (A) is due to the high sensitivity to a small change in frequency. It is noted that the frequency has fifth power in accordance with GEM eq. 3.

Conclusion

- The effect of varying sizes of graphite particulates on composites has been evaluated for storage and loss moduli. Results for composites C2 showed improved damping behavior by 50 % over the other composites for the entire test temperature range employed.
- Improved performance in loss factor was noticed in C2 composites, which can be attributed to aluminum carbide formation at the interface, and threshold modulus (volume to the surface of the particulates) that observed in C2 than other composites C1 and C2.
- Generalized Experimental Model (GEM) has been developed to account for multiple influencing parameters on damping capacity. Exponent A provides a significant finding in damping behavior. It is inferred that, if the A is less than 0.7, it indicates the improved damping behavior whereas if A is greater than 0.7 gives the poor damping behavior.

- GEM provides a distinct single dimensionless number (A) which indicates the characteristic behavior of composites. GEM emphasizes the least influence of graphite particulate sizes, which are employed in this work; it is because of the average behavior predicted by the model.
- GEM model should be attempted to apply for bigger size particles of graphite reinforcement.

Acknowledgements

Author thanks Naval Research Board-Defense Research and Development Organization for sponsoring the project.

Conflicts of interest
The authors declare that they have no conflicts of interest.

Keywords

AA7075-Gr composite, hot forging, heat treatment, loss factor, dimensionless model.

Received: 26 August 2020
Revised: 4 December 2020
Accepted: 10 January 2021

References

1. Aoba, T.; Kobayashi, M.; Miura, H.; *Mater. Sci. Eng. A*, **2017**, *700*, 220.
2. Li, J. F.; Peng, Z.W.; Li, C. X.; Jia, Z. Q.; Chen, W. J.; Zheng, Z. Q.; *Trans. Nonferrous Met. Soc. China*, **2008**, *18*, 755.
3. Imran, M.; Khan, A. R.; *J. Mater. Res. Technol.*, **2019**, *8(3)*, 3347.
4. Zhang, J.; Perez, R.; Gupta, J. M.; Lavernia, E. J.; *Scr. Metall. Mater.*, **1993**, *28*, 91.
5. Lu, H.; Xianping, W.; Zhang, T.; Zhijun, C.; Qianfeng F.; *Materials*, **2009**, 2, 958.
6. Zhang, J.; Perez, R. J.; Gupta, M.; Lavernia, E. J.; *J. Mater. Sci.*, **1993**, 28, 2395.
7. Rohatgi, P. K.; Nath, D.; Singh, S. S.; Keshavaram, B. N.; *J. Mater. Sci.*, **1994**, *29*, 5975.
8. Zhang, J.; Parez, R. J.; Lavernia, E. J.; *Acta Metall. Mater.*, **1994**, *42(2)*, 395.
9. Deng, C. F.; Wang, D. Z.; Zhang, X. X.; Ma, Y. X.; *Mater. Lett.*, **2007**, *61*, 3229.
10. Chung, D. L.; *J. Mater. Sci.*, **2001**, *36*, 5733.
11. Jinhai, G.; Zhang, X.; Mingyuan, G.; Min, G.; Wang, X.; *J. Alloys Compd.*, **2004**, *372*, 304.
12. Kenneth, K. A. Adetomilola, V. F.; *Eng. Sci. Technol. an Int. J.*, **2018**, *21*, 798.
13. Wu, G. H.; Dou, Z. Y.; Jiang, L. T.; Cao: J. H.; *Mater. Lett.*, **2006**, *60*, 2945.
14. Wei, J. N.; Wang, D. Y.; Xie, W. J.; Luo, J. L.; Han, F. S.; *Phys. Lett. A*, **2007**, *366*, 134.
15. Wei, J. N.; Cheng, H. F.; Zhang, Y. F.; Han, F. S.; Zhou, Z. C.; Shui, Z. P.; *Mater. Sci. Eng. A*, **2002**, *325*, 444.
16. Polmear, I. J.; Light Alloys from Traditional Alloys to Nano-crystals; 4th ed.; Melbourne, Australia, **2006**, pp. 105-107.
17. ASM Metals Handbook, Forming and Forging, Vol.14, 9th ed., Metals Park, Ohio, **1988**, pp. 530-560.
18. ASM Metal Handbook, Metallography and Microstructures, Vol. 09, **2004**, pp. 1719-1720.
19. ASM Metals Handbook, Heat Treating, Vol.4, 10th Ed., Metals Park, Ohio, **1991**, pp. 1861-1960.
20. ASTM E756-05, Standard Test Method for Measuring Vibration-Damping Properties of Materials, West Conshocken, **2017**, pp.1-14.

Appendix

A.1. Formulation of generalized experimental model (GEM) for loss factor

$$\tan\delta = f(\rho_c^{\,a}, F_m^{\,b}, P_p^{\,c}, E_c^{\,d}, R_d^{\,e}, t_a^{\,f}, H_b^{\,g}, a^h, f^{\,i}, t^{\,j}, T^k, \lambda^l) \quad (4)$$

The corresponding dimensional equation would be

$$M^0L^0T^0\theta^0 = [(M^1L^{-3})^a, (0)^b, (0)^c, (M^1L^{-1}T^{-2})^d, (0)^e, (T^1)^f, (M^1L^{-1}T^{-2})^g, (L^1)^h, (T^{-1})^i, (T^1)^j, (\theta^1)^k, (T^{-1}\theta^1)^l] \quad (5)$$

where, zero indicates no dimensional form for the parameter. If the equation is to be dimensionally homogeneous, the following relationship among the exponents obtained:

$$\text{For M:} \quad 0 = a + d + g \quad (6)$$
$$\text{For L:} \quad 0 = -3a - d - g + h \quad (7)$$
$$\text{For T:} \quad 0 = -2d + f - 2g - i + j - l \quad (8)$$
$$\text{For } \theta\text{:} \quad 0 = k + l \quad (9)$$

The above equations are solved and d, h, i and l indices are eliminated. There are twelve unknowns and four primary dimensions so there will be eight pi-terms that are in line with Buckingham's Pi theorem:

$$\tan\delta = f(\rho_c^{\,a}, F_m^{\,b}, P_p^{\,c}, E_c^{\,-(a+g)}, R_d^{\,e}, t_a^{\,f}, H_b^{\,g}, a^{2a}, f^{\,(2a+f+j+k)}, t^j, T^k, \lambda^{-k}) \quad (10)$$

$$\tan\delta = f\left[\left(\frac{\rho_c f^2 a^2}{E_c}\right)^a, (F_m)^b, (P_p)^c, (R_d)^e, (t_a f)^f, \left(\frac{H_b}{E_c}\right)^g, (ft)^j, \left(\frac{fT}{\lambda}\right)^k\right] \quad (11)$$

$$\tan\delta = \varphi\left[\left(\frac{\rho_c f^2 a^2 H_b}{E_c^2}\right)(F_m P_p R_d)(t_a f)(f t)\left(\frac{f T}{\lambda}\right)\right] \quad (12)$$

$$\tan\delta = \varphi\left[\frac{\rho_c\, f^5\, a^2 H_b\, t_a\, t\, T\, F_m\, P_p\, R_d}{E_c^2\, \lambda}\right]^A \quad (13)$$

$$\tan\delta = \varphi(Z)^A \quad (14)$$

Author biography

Dr. N. B. Dhokey received Ph.D. from V.N.I.T Nagpur in 2007 and M. Tech. (Process Metallurgy) in 1995 from I.I.T. Mumbai. Presently he is working as Professor in Department of Metallurgical Engineering, College of Engineering Pune (India). He has published more than 110 papers in National and International Journal and conferences. He has 26 years of teaching experience including 6 years industrial experience in Steel plant. His main area of research is Synthesis of alloys, Powder Metallurgy, Cryogenic treatment of materials and Tribology of materials.